

Temperature-Dependent Phase Behavior of Polyelectrolyte–Mixed Micelle Systems[†]Anil Kumar,[‡] Paul L. Dubin,* Michael J. Herson, Yajuan Li, and Werner Jaeger[§]

Department of Chemistry, University of Massachusetts at Amherst, Amherst, Massachusetts 01003

Received: November 29, 2006; In Final Form: April 27, 2007

The effect of temperature on the phase behavior of a polycation–anionic/nonionic mixed micelle system, poly(dimethyldiallylammonium chloride)–sodium dodecylsulfate/Triton X-100, was studied over a wide range of surfactant compositions, ionic strengths, and polycation molecular weights using turbidimetry and dynamic light scattering. Soluble complexes become biphasic upon heating through either liquid–liquid (coacervation) or liquid–solid (precipitation) separation. The biphasic boundary comprises two regions: a coacervate domain exhibiting a lower critical solution temperature and a second superimposed domain in which either solids or very dense and viscous fluids are formed upon heating. The position of the first region is symmetrically centered around conditions corresponding to charge neutralization of complexes and their aggregates at incipient phase separation. The second region, observed at high micelle charge, corresponds to the collapse of polycation onto micelle surfaces and expulsion of counterions and can produce either dense coacervate or precipitate. The two regions exhibit different dependences on ionic strength, polyelectrolyte molecular weight, and concentration, from which inferences about the mechanisms of phase separation may be drawn. Preliminary observations of the dense liquid phases isolated after coacervation disclose a number of interesting optical and rheological properties, possibly arising from shear-induced phase separation.

Introduction

The interaction of oppositely charged polyelectrolytes can lead to soluble complexes or precipitates.^{1,2} Intermediate between these two states are complex coacervates,³ dense liquid phases much more concentrated in macroions than soluble complexes but more solvated than precipitates. Similar phase transitions can be observed in systems of polyelectrolytes with small, oppositely charged colloids, including proteins,⁴ dendrimers,⁵ and micelles^{6,7} all of which may exhibit liquid–liquid-phase separation. Coacervation between polyelectrolytes and surfactants may occur in cosmetic formulations,⁸ while protein–polyelectrolyte coacervation has been studied in the context of food systems⁹ and may also be relevant to some biological phenomena. The fact that coacervation appears to have little effect on the structure of proteins¹⁰ or micelles¹¹ leads to intriguing possibilities in the fields of protein separation,^{12,13} immobilized enzymes,¹⁴ and immobilized detergency.¹⁵ These applications and implications have motivated studies of coacervation and the factors that influence it.

Stoichiometric complexation in polyelectrolyte–surfactant systems has been reported,¹⁶ and the formation of stoichiometrically well-defined (solid) complexes^{17,18} tends to occur under conditions of strong binding when free surfactant and free polyelectrolyte (PE) cannot coexist. Such strong binding, characteristic of the interaction of ionic surfactants with oppositely charged PE in pure water, can be attenuated by the use of mixed anionic–nonionic micelles, making it possible to establish

regimes of soluble complex formation prior to phase separation, in turn leading to a better understanding of the coacervation process. PE–micelle interactions dominate over interactions with monomeric surfactant in part because of the typically low cmc of ionic–nonionic surfactant systems (in the present case about 3 orders of magnitude below the bulk surfactant concentration). The predominance of PE–micelle interaction is manifested in (1) the appearance of a critical micelle charge density for complexation,^{6,7} (2) the quantitative retention of solubilization by polyelectrolyte-bound micelles in solution or coacervates,¹⁵ and (3) direct cryo-TEM observation of PE–complexed micelles.^{11a}

Polyelectrolyte–micelle systems facilitate experimental tests of theories for the electrostatic interaction between PE's and oppositely charged colloids,^{19,20} in particular providing the only experimental evidence in support of the theoretically observed²⁰ minimal colloid surface charge density σ_c required for binding:

$$\sigma_c \sim \xi \kappa^a \quad (1)$$

Here ξ is the PE linear charge density and κ is the Debye–Hückel parameter. These systems also provide a good model for elucidating the dependence of PE–colloid coacervation on system variables such as colloid charge, polyelectrolyte (PE) MW, colloid:PE stoichiometry, and ionic strength (I).^{6,7} We have focused in particular on the polycation poly(dimethyldiallylammonium chloride) (PDADMAC), whose linear charge density seems particularly conducive to coacervation, using narrow MW distribution samples to observe the relevant phase transitions, thus avoiding much of the broadening due to system polydispersity. The surfactant system of sodium dodecyl sulfate (SDS) and Triton X-100 (TX100) allows for simple adjustment of micelle surface charge density,^{21,22} with analogs of the latter allowing for variation of average micelle head group size.

Although polyelectrolyte–colloid coacervation can be formed over a wide range of conditions, the influence of temperature

[†] Part of the special issue “International Symposium on Polyelectrolytes (2006)”.

* To whom correspondence should be addressed. Tel: (413) 577-4167. Fax: (413) 545-4490. E-mail: dubin@chem.umass.edu.

[‡] Permanent address: Post Graduate Department of Chemistry, College of Commerce, Patna-20, India-800020.

[§] Present address: Fraunhofer Institute of Applied Polymer Research, D-14476 Potsdam-Golm, Germany.

has not yet been reported. The conditions required for protein–polyelectrolyte coacervation (expressed as a critical pH) were found to be remarkably independent of temperature in the range 20–50 °C.⁴ Coacervation of PDADMAC with SDS/TX100 micelles was found to have essentially no enthalpy change.²³ But, phase separation with increase in temperature had been observed previously.²⁴ Thus, it was not entirely unexpected when we serendipitously observed a phase transition between 2 °C and body temperature for coacervates prepared at room temperature. Since control of phase state could be important in several applications, we were prompted to investigate this effect in more detail. Here, we report on the influence of molecular weight of polyelectrolyte (MW), salt concentration (I), and polymer concentration (C_p) on the temperature-induced phase behavior PDADMAC/TX100-SDS. Turbidimetric titrations were used to identify regions of Y corresponding to the formation of soluble complexes, coacervate, or precipitate. Dynamic light scattering was employed to characterize the system in all three regimes. Since all three of these states could give rise to turbidity, clear distinctions among them are only possible after high-speed centrifugation. The optically clear dense fluids obtained after centrifugation we define as “coacervates” (in the literature “coacervation” typically refers to the formation of a metastable suspension of this fluid in the dilute phase). We also make some preliminary observations of the interesting rheological and optical properties of the coacervates.

Experimental Section

Materials. Two samples of Poly(diallyldimethylammonium chloride) (PDADMAC) were prepared by free radical aqueous polymerization of diallylmethylammonium chloride.²⁵ The weight average molecular weights (M_w) of the two purified lyophilized polymers were determined by light scattering as 2.19×10^5 and 7.00×10^5 , but the samples will be referred to according to their number averages (from membrane osmometry) $M_n = 1.41 \times 10^5$ and 4.60×10^5 . Triton X-100 (TX100) and sodium dodecyl sulfate (SDS, purity >99%) were purchased from Aldrich, and NaCl was from Fisher. Monodisperse hexaoxyethylene dodecyl ether ($C_{12}E_8$) was from Nikkol Chemical Co. (Tokyo), while a commercial sample with headgroup polydispersity was a gift from Shiseido Corp. (Yokohama, Japan). All were used without further purification. Milli-Q water was used in all experiments.

Turbidimetric Titrations. Turbidimetric titrations were carried out by adding 60 mM SDS in 0.40 M NaCl with continuous stirring to solutions of PDADMAC in 20 mM TX100, also in 0.4 M NaCl, with initial polymer concentrations 1 or 3 g/L, respectively, to bring the solution to different mole fractions of SDS (Y). Y is defined as

$$Y = [\text{SDS}] / \{[\text{SDS}] + [\text{TX100}]\} \quad (2)$$

which is proportional to the average mixed micelle surface charge density, i.e., σ in eq 1. Turbidity, reported as $100 - \% T$ ($\pm 0.1\% T$), was measured using a Brinkmann PC 800 colorimeter ($\lambda = 420$ nm) equipped with a 2.0 cm path length fiber-optics probe. The temperature was controlled by a circulating water bath (± 0.2 °C). Turbidity values were recorded when the meter response was constant for 2 min. All measured values were corrected by subtracting the turbidity of a polymer-free blank. Duplicate titrations gave reproducible results.

Dynamic Light Scattering (DLS). DLS measurements were carried out mainly on preacervate solutions at scattering angle 90° at temperatures from 5 to 36 °C ± 0.5 °C with an ALV instrument equipped with a model 5000 Multi-tau digital

correlator and employing a 3 W Ar-ion laser source operating at 514 nm. Samples were prepared in 0.40 M NaCl containing 3 g/L PDADMAC (1.41×10^5) and 20 mM TX100 adjusted with 60 mM SDS to desired Y values. The samples were stirred at least 2 h before measurements and filtered with Whatman (0.2 μm) filters prior to measurements. The correlation functions of the scattering data were analyzed via the method of regularization (CONTIN)²⁶ and then used to determine the diffusion coefficients (D). The diffusion coefficient D can be converted into hydrodynamic radii using the Stokes–Einstein equation

$$R_h = kT/6\pi\eta D \quad (3)$$

where k is the Boltzmann constant, T is the absolute temperature, and η is the solvent viscosity, here taken as that of water.

Coacervate Separation. Turbidimetric titrations were carried out at constant temperature by adding SDS to 3 g/L (1.41×10^5) PDADMAC and 20 mM TX100. Titrations were stopped at desired Y values corresponding to biphasic domains III or V (see below), and the resultant suspensions were stirred for 15 min. For experiments not at ambient temperature (22 °C), the solutions were kept in a controlled temperature water bath for 1 h. The strongly turbid samples were centrifuged at least 2 h at 3500 rpm at the temperature of preparation, to yield an upper dilute phase and lower dense phase (“coacervate”), which was, depending on the value of Y and the temperature, (a) a somewhat viscous optically clear fluid, (b) a translucent and gel-like fluid, or (c) a white solid. In cases a and b, both phases were separated for further examination.

Results and Discussion

Turbidimetric Titration: Presence of Different Characteristic Domains. Gradual addition of ionic surfactant to a mixture containing an oppositely charged polyelectrolyte (PE) and a nonionic surfactant (well above the cmc) corresponds to a continuous increase in micelle surface charge density. Monitoring the turbidity with high precision (± 0.1 transmittance units) facilitates the detection of soluble complexes and their subsequent aggregation, as well as macroscopic phase transitions, including liquid–liquid-phase separation.^{6,7} Previous studies⁷ showed that such coacervation is highly dependent on the mole fraction of anionic surfactant (Y), the salt concentration (I), the polymer molecular weight (MW), the polymer concentration (C_p), and the related bulk stoichiometry, here expressed as the weight ratio of total surfactant:polymer (r). For 0.40 M NaCl, $C_p = 1$ g/L, coacervation at room temperature was not observed when $M_n \leq 2.16 \times 10^5$. Therefore, the concentration of PDADMAC ($M_n = 1.41 \times 10^5$) was increased to 3 g/L. The corresponding turbidimetric titration curve shown in Figure 1 allows for the identification of five domains or regions, corresponding to either colloidal solutions or biphasic systems. The turbidity τ (here defined for convenience as $100 - \% T$, which is linear with the true turbidity for $T > 0.9$) is constant and very small in region I, until Y attains a critical value (Y_c) of 0.23; beyond this point, the turbidity increases gradually (region II). Numerous studies^{27–29} have demonstrated that polyelectrolyte–micelle interactions are negligible below this Y_c , regardless of total surfactant concentration, confirming as noted above that the polycation interacts with the mixed micelles and not monomeric surfactant. It has also been clearly established that Y_c is independent of C_p , MW, or r and uniquely determined by I . Above Y_c , the gradual increase in τ corresponds to the formation of intrapolymer soluble complexes and their

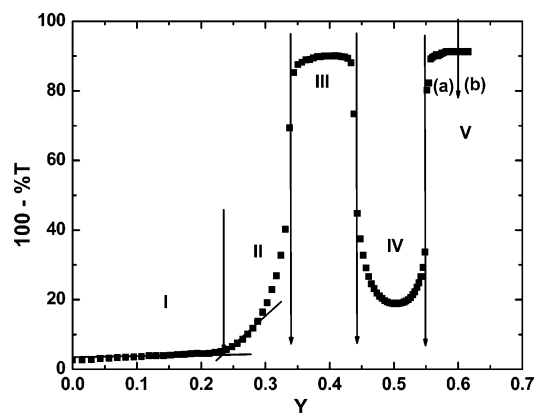


Figure 1. Characteristic regions of turbidimetric titration: PDADMAC (1.41×10^5 , 3 g/L), in 20 mM TX100 and 0.4 M NaCl, is titrated with 60 mM SDS in 0.4 M NaCl to vary the mole fraction of SDS (Y) at 22 °C. The vertical arrows indicate the phase transitions from noninteracting solution (I) to soluble complex (excess polycation) (II), to coacervates (III), to soluble complexes and aggregates (excess micelle) (IV), and finally to dense coacervates (V(a)) and precipitate (V(b)).

higher order aggregates. A subsequent abrupt and dramatic increase in τ occurs at $Y = 0.32$, beyond which coacervation is demonstrated by the formation of two liquid phases upon centrifugation; this is designated as $Y_{\phi 1}$. Further addition of SDS causes the coacervate to redissolve at $Y_{\phi 2}$ accompanied by a decrease in τ , attaining a second plateau but one of significantly higher τ than at $Y < Y_c$. Thus, the interval between $Y_{\phi 1}$ and $Y_{\phi 2}$ is the first coacervation region, hereinafter referred to as “III”. The electrophoretic mobility of soluble complexes is positive at $Y_c < Y < Y_{\phi 1}$ and negative for $Y > Y_{\phi 2}$, indicating that coacervation is inhibited when soluble complexes are not close to electroneutrality.⁶ The subsequent sharp increase in turbidity at $Y \approx 0.55$ corresponds to a second coacervation domain as demonstrated by the formation of a dense and viscous lower liquid phase (“V”) upon centrifugation. However, at $Y > 0.60$, solid–liquid separation (precipitation) was observed. The domains of the five states are thus denoted as noninteracting (I), positively charged soluble complex (II), coacervate (III), negatively charged soluble complex (IV), and a second phase separation regime (V). Previously, this domain was thought to correspond to precipitation and was therefore denoted by Y_p . In this work, we found that this region often corresponded to a second coacervate essentially continuous with eventual precipitation; in the absence of a well-defined boundary in these cases, we designate the corresponding regimes as V(a) and V(b).

The progression described above arises from enhanced binding of micelles with increasing surface charge density to polycation. According to Veis and Aranyi,³⁰ complex coacervation between oppositely charged macromolecules involves first the aggregation of macroions by electrostatic interactions to form neutral aggregates of low configurational entropy, followed by their rearrangement to form coacervate. This corresponds here to region III, in which the number of micelles bound/polymer chain, n , multiplied by the charge/micelle, Z_m , begins to compensate for the charge/polycation. Subsequent increase in both n and Z_m leads to charge overcompensation, and complexes with net negative charge undergo dissolution due to intermacroionic repulsion, leading to the soluble complex region IV. In this region it is also possible that intramacroionic repulsion leads to a decrease in n . At $Y > 0.56$, the second coacervation region may be attributed to the tight binding to polyelectrolyte of mixed micelles with very high charge density. Pursuant to the consequent loss of counterions and hydration,

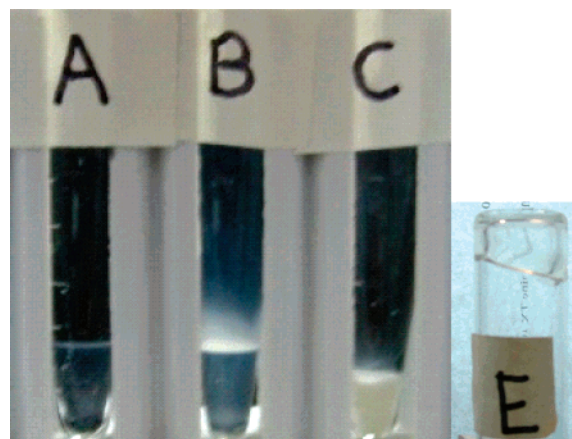


Figure 2. Systems obtained by centrifugation of 1.41×10^5 PDADMAC (3 g/L + SDS-TX100, after adjustment to $Y = 0.38$ (A), 0.57 (B), and 0.61 (C); centrifugation temperature 22 °C for (A) and 27 °C for (B) and (C)). Volumes before centrifugation: 5 mL (A); 15 mL (B); 10 mL (C). Volumes of lower and upper phases: 0.4, 4.6 mL (A); 0.3, 14.7 mL (B); 0.2, 9.8 mL (C). Some upper phase was discarded for (B) and (C). Actual yields of dense phase (v:v): 8% (A); 2% (B); 2% (C). (E) displays the viscosity of the coacervate from (B) (inverted for several minutes before image).

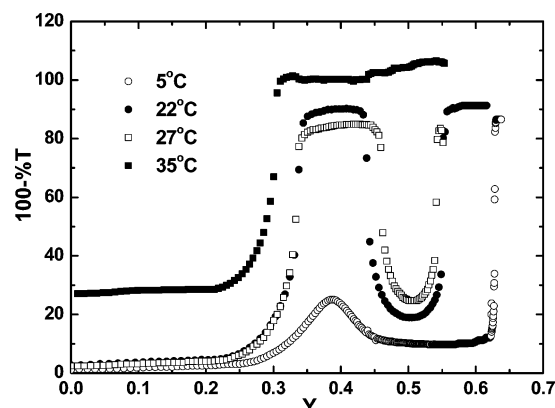


Figure 3. Turbidimetric titration curves at 5, 22, 27, and 35 °C, with all other conditions as in Figure 1 (35 °C plot shifted up by 20 for clarity of presentation).

dense coacervation [V(a)] followed by precipitation [V(b)] occurs. The three states of phase separation, corresponding to III, V(a), and V(b), initially formed as metastable suspensions, are identified by the appearance of the lower phase after centrifugation in Figure 2.

Temperature Dependence. The effect of temperature is first illustrated through turbidimetric titrations carried out at low temperature (5 °C), ambient (22 or 27 °C), or elevated temperature (35 °C), shown in Figure 3. Notable is the fact that the transition from noninteracting state to soluble complex at “ Y_c ” ≈ 0.23 is at most weakly dependent on temperature. At $T = 22$ °C, centrifugation subsequent to region IV at $Y = 0.57$ gives two liquids (dilute phase and coacervate) and at $Y = 0.61$ gives dilute phase and solid. At 35 °C (to be discussed in more detail below), the system becomes and remains biphasic shortly after Y_c and, thus, region IV appears to be absent. In contrast, at 5 °C, phase separation is delayed, the coacervation region (III) is absent, and only solid–liquid phase separation was observed at $Y = 0.64$; i.e., region V(b) appears without V(a). It is evident that at fixed $Y = \text{ca. } 0.38$, coacervation will occur somewhere between 5 and 22 °C. In fact, this observation first occurred adventitiously when solutions at similar conditions were merely held. It should be pointed out that the appearance

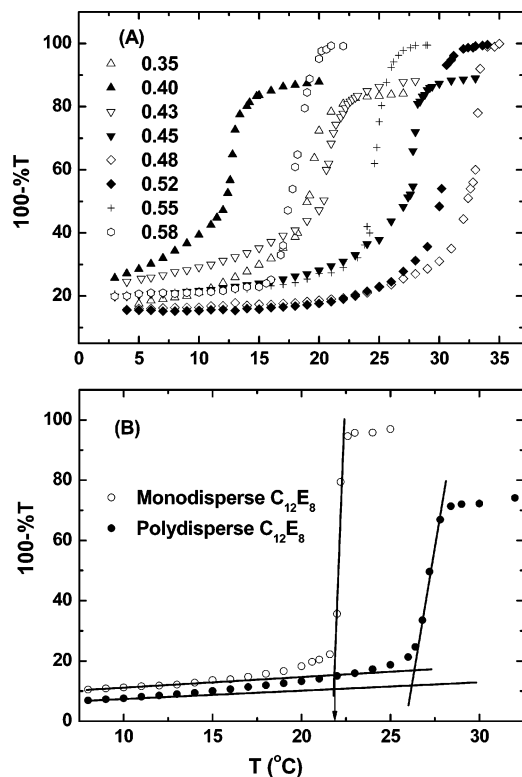


Figure 4. Temperature dependence of turbidity for PDADMAC (1.41×10^5 , $C_p = 3$ g/L) + SDS/nonionic mixed micelles in 0.4 M NaCl: (A) SDS/TX-100 at various Y values; (B) SDS/C₁₂E₈ (monodisperse and polydisperse), $Y = 0.40$. Also shown: operational definition of T_Φ , used to determine data points for the phase boundary of Figure 6.

of a critical temperature for coacervation (T_Φ) does not arise directly from transitions of the surfactant. The cloud point of the surfactant system at $Y = 0.38$ is above 65 °C, much higher than the values of T_Φ . The polyelectrolyte-free system freezes at -3 °C, while the coacervates freeze at -7 °C. Finally, coacervates are far more viscous than polyelectrolyte-free solutions of identical surfactant concentration.

More quantitative measurement of this T_Φ is illustrated by Figure 4. The curve exhibits sigmoidal shape with an abrupt increase at a threshold temperature corresponding to phase separation, allowing an empirical definition of T_Φ as the intercept of the initial linear portion of the curve with the tangent to the rapidly increasing portion of the curve, as shown in Figure 4B for $Y = 0.40$. When T is below T_Φ , the mixed solution is transparent and the turbidity τ is small and increases gradually. This gradual increase in τ may indicate progressive formation of intrapolymer soluble complexes. In the vicinity of T_Φ , the turbidity increases rapidly, which may come from the aggregation of intrapolymer complexes into interpolymer complexes. For $T > T_\Phi$, τ exhibits a rapid increase (the subsequent leveling off cannot be interpreted since the amount of light reaching the detector becomes unmeasurably small). Figure 4B shows results for a system in which surfactant heterogeneity is minimized by replacing TX100 with a monodisperse analog, C₁₂E₈. Broadening of the transition is increased when the nonionic headgroup becomes polydisperse (commercial C₁₂E₈). Thus, coacervation at $T > T_\Phi$ (demonstrated by the formation of two liquid phases upon centrifugation) is a true liquid–liquid-phase transition broadened only by system polydispersity.

While the precise nature of the transition at T_Φ remains to be elucidated, two models of macromolecular liquid–liquid-phase separation come to mind: the historically familiar coacervation of oppositely charged polyelectrolytes^{30–35} and

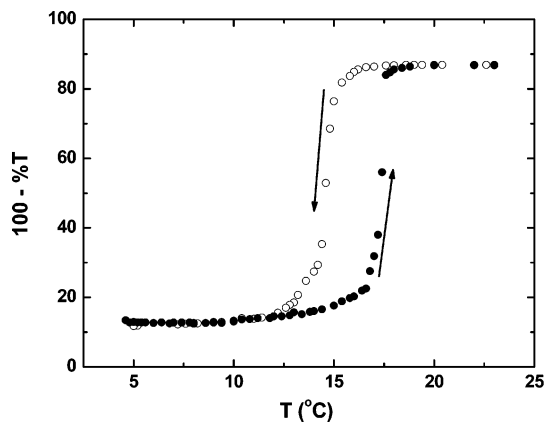


Figure 5. Hysteresis at $Y = 0.61$. T_Φ (heating) = 16.8 °C, and T_Φ (cooling) = 14.5 °C.

temperature-induced phase separation for polymers in poor solvents.³⁶ The former has rarely been identified as a true phase transition, being typically broadened by system polydispersity, and does not appear to have any consistent temperature dependence. Temperature effects for the latter have been the subject of a rigorous thermodynamic analysis but in the context of simple polymer–solvent binary mixtures. Like the first case, phase separation in our system is entropy-driven (see below), but reduction in MW polydispersity and surfactant heterogeneity facilitates the observation of well-defined transitions (Figure 4B), similar to those seen for polyelectrolyte–protein coacervation induced by a change of only ca. 0.02 pH units.⁴ The curves of Figure 4 were fully reversible and highly reproducible, yielding T_Φ to ± 0.5 °C. However, at $Y > 0.58$, where the dense phase is solid, a hysteresis appears as shown in Figure 5. This does not appear to be a kinetic effect since the redissolution curve (decreasing temperature) was highly reproducible, but its existence at all conditions has not been verified. The symmetry and position of the curves in Figure 4 clearly vary nonmonotonically with Y , for reasons to be presented in the subsequent section.

The dependence of T_Φ on Y is shown as the phase boundaries of Figure 6A for PE MW's and concentrations of 1.41×10^5 and 3 g/L. It can be pointed out that this phase boundary could also be generated by measuring Y_Φ at different fixed temperatures, and the result of one such turbidimetric titration, presented in Figure 1, constitutes one of the data points in Figure 6A. A prominent feature of Figure 6A is a well-defined minimum at a lower critical solution temperature (LCST). (No UCST could be observed as the solutions freeze prior to phase separation.) We denote this LCST as T^* and the corresponding micelle composition as Y^* . It is important to note that this Y^* is identical with the local maximum in τ for noncoacervating conditions (e.g., at $T < T_\Phi$ in Figure 4) or to the point of maximum coacervation for the turbidimetric titration curve of Figure 1, all three corresponding to conditions for charge neutrality of the PE–micelle complex or aggregates thereof.

The temperature-dependent turbidities of Figure 4A contain additional information beyond the phase boundary of Figure 6A. For Y in the vicinity of Y^* , the turbidity τ increases steeply with approach to T_Φ , while departures of Y from Y^* in either direction lead to a marked decrease in the slope of $d\tau/dT$. Thus, systems that display quite different values of T_Φ can generate $\tau(T)$ curves of very similar shape if the absolute values of $|Y - Y^*|$ are similar. This symmetry with respect to Y^* is important and will be discussed below.

To confirm the phase boundary of Figure 6A, turbidimetric titrations were carried out at 5 and 35 °C corresponding to the

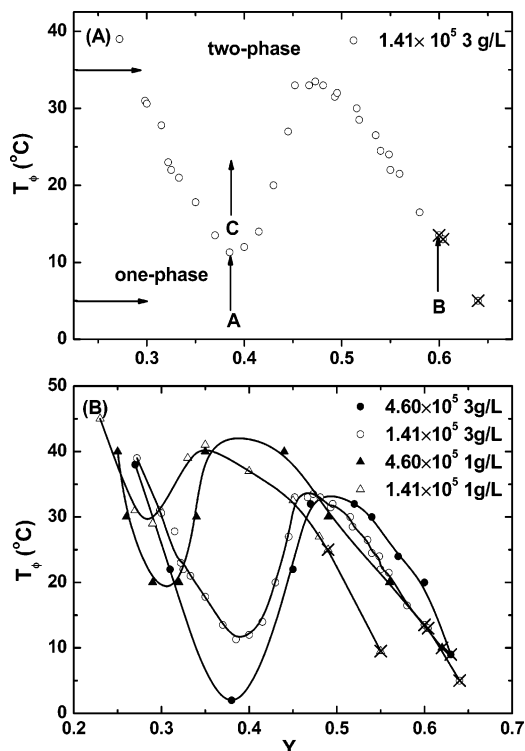


Figure 6. (A) Phase boundary constructed from data in Figure 4. The data point at $Y = 0.32$ and $T_\phi = 22$ °C was obtained from the turbidimetric titration of Figure 1. Solid–liquid separation occurs under conditions denoted by “x”. Horizontal arrows correspond to paths of turbidimetric titrations at 5 and 35 °C shown in Figure 3. Vertical arrows A and B show conditions for temperature-dependent DLS (see Figure 7). Arrow C corresponds to the effect of temperature on coacervate prepared at 22 °C leading to second phase separation (see Figure 10). (B) Effect of polymer MW and concentration on phase boundaries.

horizontal arrows shown in Figure 6A. The coacervation domain vanishes at 5 °C, and the system progresses directly from monophasic to liquid–solid phase separation at $Y \approx 0.64$ (this point is indicated by the solid crosses in Figure 6A). However, at 35 °C the biphasic region extends beyond $Y = 0.27$ apparently with no indication of a second soluble complex regime IV; instead, there appears to be a transition from coacervate to precipitate at $Y \approx 0.57$. This transition cannot be observed turbidimetrically but is disclosed by comparison of centrifugates after adjustment of Y . Figure 3 verifies that the coacervation corresponding to region III cannot occur below the LCST.

Structural information on complexes and coacervates from dynamic light scattering can help to understand the nature of the phase transition. As shown in Figure 7A for the case of $Y = Y^* = 0.38$, unbound micelles ($R_h = 5$ nm) are seen throughout the experimental range, along with intrapolymer complexes ($R_h = 25$ nm). At $T > 7.5$ °C, interpolymer (multipolymer) complexes appear in the range of $R_h = 100$ nm and increase in size until 13.5 °C, where particles with $R_h > 500$ nm appear. Similarly, $Y = 0.40$ shows strong increases in turbidity as a function of T prior to the onset of phase separation. In summary, there are four species that can be identified in Figure 7A: (1) unbound micelles, with diffusion coefficients identical with those seen in the absence of polymer; (2) intrapolymer complexes, with apparent dimensions 18–25 nm similar to those of free polymer; (3) “aggregate” species with apparent radii on the order of 100 nm, present in the one-phase regime but exhibiting somewhat higher turbidities, which may thus be identified as interpolymer complexes; (4) ca. 500 nm objects appearing abruptly at $T > 14$ °C, corresponding

to coacervate droplets which can be separated into well-defined phases by centrifugation.

While Figure 6 gives T_ϕ at $Y = 0.38$ as 10.8 ± 0.5 °C for $M_n = 1.41 \times 10^5$ and $C_p = 3$ g/L, Figure 7A for identical conditions of PE concentration and MW shows a marked discontinuity at 13.5 ± 0.5 °C. The features of the temperature dependence of DLS scattering intensity, shown in Figure 8, differ even further with a sharp maximum at 12 °C. The size of coacervates droplets leads to a large scattering dissymmetry ratio due to interference effects, so their 90° scattering is weak, and this strongly affects the DLS results. Their global scattering (turbidity) is large, so T_ϕ from turbidity is a good measure of the initial formation of coacervates. On the other hand, the scattering at 90° is dominated by smaller species, particularly soluble complexes, which continue to be seen above T_ϕ (this explains why the small micelles are detected by DLS even for highly turbid samples). At 12 °C, soluble complexes are being depleted to form coacervates, giving rise to the maximum in 90° scattering intensity at 12 °C. Continued depletion of soluble complex allows coacervates droplets to be detected at $T > 14$ °C. Taken together, Figure 7A,B indicates that the maximum size for soluble aggregates is somewhere between 100 and 400 nm.

Our discussion of Figure 6A begins with the rather symmetrical regions around Y^* . Previous work⁶ indicates a transition from positively to negatively charged soluble complexes near the point of incipient phase separation as the system progresses from regime II to IV. This provides strong evidence that the point of maximum coacervation $Y^* = 0.38$ for this ionic strength and PE concentration corresponds to the condition of zero net charge of soluble complexes, which promotes the formation of aggregates, seen for example in Figure 7A between 10 and 15 °C. The LCST seen in Figure 6A corresponding to conditions of incipient liquid–liquid phase separation thus signals the formation of nearly electrically neutral polyelectrolyte–micelle complexes.⁶ This condition may be described by

$$Z_T = Z_p - nZ_m \approx 0 \quad (4)$$

i.e. the number of micelles/polymer chain multiplied by the (Y -dependent) charge/micelle is nearly equal to the polymer charge. This is consistent with the symmetry around Y^* of the dT/dY slopes: deviations from charge neutrality similar in magnitude, if not in sign, arise rather equally when micelle charge deviates in either direction from Y^* , and the concomitant deviations from complex charge neutrality equally reduce pre-coacervate higher order aggregation. Accordingly, the LCST curve is symmetrical around Y^* . Small deviations from $Z_T = 0$ still permit aggregation, either by polarization (a transiently micelle-rich domain of one complex attracted to a transiently micelle-poor domain of another) or by disproportionation (the formation of a subpopulation of neutral complexes by the unequal sharing of micelles within a population that is not globally electroneutral). Even with these effects, coacervation is constrained when Y deviates from Y^* , thus expanding the one-phase region (elevating T_ϕ).

To pursue the charge-neutrality hypothesis further, we recognize that n has both energetic and stoichiometric components. At fixed ionic strength, energetic contributions to micelle binding depend only on Y but clearly in a nonmonotonic way, since $n = 0$ when $Y < Y_c$. Although this nonmonotonic dependence leads to the appearance of phase-transition-like behavior (a rapid increase in binding as a function of Y) at Y_c , the system still follows isotherm-like behavior: at fixed C_p , Y , and I , n is a function of total added surfactant C_s , reaching

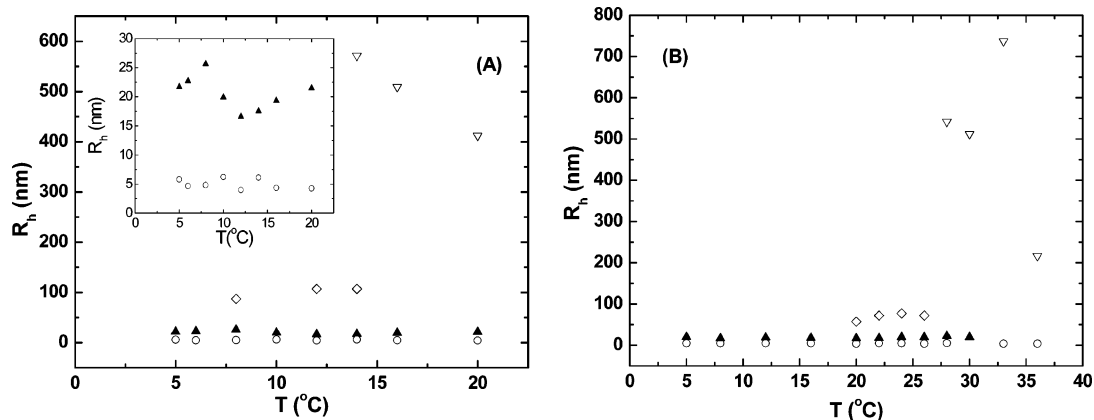


Figure 7. Apparent Stokes radii from DLS as a function of temperature for $Y = 0.38$ (A) and $Y = 0.56$ (B), corresponding to vertical lines (A) and (B) in Figure 6. Inset: Expansion of data points corresponding to (○) free micelles and (▲) soluble complexes.

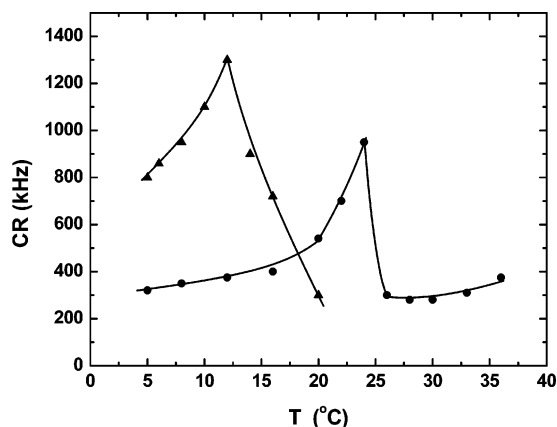


Figure 8. Temperature dependence of DLS 90° count rate (kHz): $Y = 0.38$ (▲); $Y = 0.56$ (●).

saturation at high C_S .²² As a corollary of this stoichiometry, n is generally a function of bulk stoichiometry, i.e., $C_p/C_S \cong 1/r$. This effect can be observed in Figure 6B in which polymer concentration is changed from 3 to 1 g/L for both $M_n = 1.41 \times 10^5$ and 4.60×10^5 . At lower C_p , i.e. higher r , corresponding to a larger excess of micelles, n increases, so that (see eq 4) the value of Z_m required for electroneutrality decreases, corresponding to a lower value of Y at conditions for phase separation. Such a shift is seen for both MW's in Figure 6B when C_p is decreased. Because an increase in C_p at fixed MW also increases the proximity and abundance of soluble complexes, thus facilitating aggregation, the coacervation region expands for higher C_p ; i.e., LCST moves down.

Effects of Polyelectrolyte MW and Ionic Strength. Figure 6B also shows that an increase in MW expands the biphasic region at both concentrations, lowering T_ϕ . This effect would be consistent with the polarization mechanism put forward above, but we cannot rule out the viewpoint that the complex itself behaves as a sort of polymer, with the MW influencing phase behavior through chain configurational entropy in the classical way.³⁷ While the theory of polymer phase separation³⁶ is a foundation for understanding *inter alia* LCST behavior, extension to the current system is enormously complicated by two effects. First, that thermodynamic treatment and its attendant χ parameter are inappropriate for long-range interaction where the lattice model breaks down. Second, attempts to view the complex as a type of macromolecule confront the variation in the structure of this “polymer” with the many system variables, since the number of micelles bound/PE chain n (as well as their composition) is a function of, e.g., ionic strength and Y , and n

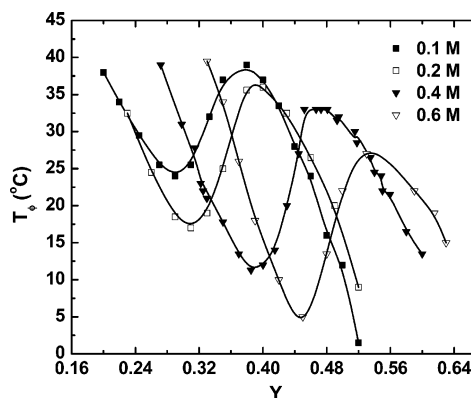


Figure 9. Effect of salt concentration on phase boundaries ($M_n = 1.41 \times 10^5$, $C_p = 3$ g/L).

and Y are clearly central parameters describing both long-range and short-range interactions in this system. Extension of classical polymer solution theory to the present case is thus an unpromising strategy. It is also noteworthy that MW has little effect on the position of Y^* , which is consistent with the stoichiometric argument used to explain the effect of C_p .

Figure 9 shows that the biphasic region expands with increased salt concentration, while LCST shifts to lower T_ϕ and larger Y ; we now offer an explanation of these three effects. With regard to the last, the screening of micelle–polyelectrolyte interactions by added salt, embodied in eq 1, can be expected to shift to larger Y all features of the various transitions in Figure 9, including Y^* . More specifically, the addition of salt could reduce the number of micelles bound per polymer chain n at any given Y and thus delay the attainment of soluble complex charge neutrality until a larger value of Y is reached.

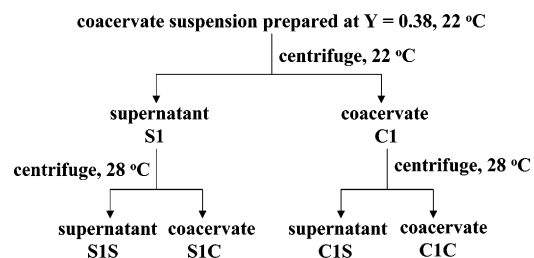
In addition to the increase in Y^* , we observe a marked decrease in T^* with added salt. While multiple arguments for this enhancement of coacervation with increased I might be imagined, we consider an indirect effect of salt, arising from the increase in Y^* concomitant with an increase in I . Although coupled increases in Y and I could cancel each others' effect on micelle–polyelectrolyte interaction, the increase in micelle surface charge density could affect the complementarity between surfactant SO_3^- headgroups and PE charge sites. To assess this effect, we examined the change in the distance between SO_3^- groups for the conditions of $Y^* = 0.38$ vs 0.46 at respectively ionic strengths of 0.4 and 0.6 M. First, we interpolated reported values of the micelle molecular weight^{38,39} to estimate the aggregation number of SDS/TX-100 at $Y^* = 0.38$ and $I = 0.4$ M as 1062; we used reported values for the micelle hydrody-

amic radius⁴⁰ along with numerical values from the Perrin equation to obtain first major and minor ellipsoidal axes of the micelle⁴¹ and then a micelle surface area of 900 nm². From this we obtained an average distance between SO₃⁻ groups d of about 1.6 nm. A companion calculation for $Y^* = 0.46$ and $I = 0.6$ gave a value of $d = 1.1$ nm. Since both of these are larger than the spacing between PDADMAC charges of about 0.6 nm, the decrease in d in 0.6 M NaCl corresponds to a higher level of geometric complementarity of polyelectrolyte and micelle charge groups. This higher efficiency of “ion-pairing” (greater proximity of N⁺ and SO₃⁻ groups) allows for more extensive counterion release with greater entropy gain. An increase in ΔS means that the contribution of $T\Delta S$ can be achieved at lower T ; i.e., T^* moves down with increasing salt concentration. However, the preservation of an entropic contribution from small ion release at high ionic strength merits further examination.

The temperature dependence of micelle–PE coacervation suggests its entropic origin, as discussed for the complexation of proteins with PE brushes by Czeslik et al.⁴² In the present case, the only source of favorable entropy is counterion release, because reduction in the available volume for micelles and PE's upon coacervation is entropically unfavorable. Since the entropy gain/ion upon release to the bulk phase is proportional to $\ln(C_{\text{local}}/C_{\text{bulk}})$, one might question the importance of this contribution as salt concentration increase. In that case, coacervation would be enthalpically driven by electrostatic attraction. But mixing calorimetry of micelles and PE for this system shows no heat at an ionic strength I of 0.4 M NaCl.²³ A somewhat related case involves the interaction between pairs of oppositely charged PE's. Schaaf and co-workers⁴³ found that, for one pair, the reaction became nearly nonenthalpic when I was increased from 150 mM to 2 M and, in fact, became endothermic for another pair when I was increased from 1 to 160 mM. Finally, as seen in Figure 9, LCST actually decreases with I , a result consistent with more favorable entropy change with added salt. These findings indicate the persistence at high ionic strength of counterion release as an entropic driver of this and related transitions.

An increase in the breadth of region III with added salt can be understood as a suppression of the repulsive interactions that inhibit the progressive association of aggregates whose net charges differ slightly from zero. This interaction, corresponding to the largest length scale relevant here, is most strongly affected by an increase in I , so that coacervation is enhanced by addition of salt. However, for PE–PE coacervation, the models advanced by both Overbeek³⁵ (direct phase separation among polyions) and by Veis (association of neutral aggregates) showed suppression of coacervation by added salt (for different reasons), an effect also consistent with the elimination of protein–PE coacervation at $I > 50$ mM reported by Burgess⁴⁴ and Kaibara et al.⁴ Figure 9 shows a more complex ionic strength effect, with either suppression, enhancement, or nonmonotonic behavior, all depending on Y . This reveals that the effect of salt is through its influence on the electroneutrality of the aggregate: increased screening promotes neutral aggregates when Y is large enough to yield negatively charged complexes; reduced screening promotes neutral aggregates when Y is low and micelle binding needs to be enhanced for charge neutrality. We note that both the long-range nature of these interactions, and the highly variable nature of the species subject to coacervation (the PE–micelle complex and aggregates thereof) precludes application of the Flory–Huggins treatment, which is applicable for short-range interactions for solutions of well-defined uncharged polymers.

SCHEME 1: Phase Transition in Coacervate and Supernatant with Increase in Temperature



Figures 6 and 9 suggest that the symmetrical LCST curve is superimposed on an additional quasi-linear phase boundary observed at larger Y and seen most prominently when the first biphasic region is shifted and suppressed, i.e., at low C_p . In sharp contrast to the first LCST boundary, this biphasic domain (previously introduced as the boundary between regions IV and V) moves to lower T upon a decrease of MW or an increase in C_p , both the reverse of effects for the first phase separation region. These effects indicate that the phase separation phenomena in region V must be different from those in region III.

Figure 2 shows that region V actually comprises two types of phase separation: (1) solid–liquid phase separation (Figure 2C), corresponding to the “×” symbols in Figure 6 and (2) formation of a concentrated and dense liquid phase (Figure 2B), corresponding to all the other symbols beyond $Y = 0.40$ in Figure 6. Figure 7B suggests that interpolymer complexes may exist prior to abrupt phase separation at $T > 25$ °C. However, the low slopes seen in Figure 4 at $Y > 0.45$, like the C_p and MW dependence, in these regions all indicate a mechanism different from the aggregation of electrically neutral complexes. The large values of Y in region V themselves (corresponding to large Z_m and n) also preclude satisfying eq 4.

As noted above, the confinement of polymer chains in coacervates and precipitates must correspond to a loss of chain configurational entropy ΔS_p , more severe for liquid–solid phase separation, in which case an increase in the volume/particle for the microions must provide a corresponding greater entropy gain ΔS_i . The unfavorable ΔS_p in region V should increase with MW, but because coacervates are more voluminous in region III V(a) (water content is about 95%), MW has relatively little effect on ΔS_p for the this LCST region but instead enhances aggregation of complexes, as discussed above. The decrease in ΔS_p in region V (water content of dense phase <66%) is more significant. While the effect of C_p in region V is not clear, it is not likely to be related to stoichiometry as its effect in region III is.

A prominent feature of region V is the juxtaposition of points corresponding to both precipitation and the second coacervation regime; in fact, we have not observed any clear point of transition between the two, suggesting that precipitation in V(b) is an enhancement of strong desolvation for coacervation region V(a). This desolvation presumably arises from counterion loss, as does coacervation in region III but at a much higher level of desolvation (66% water for coacervate V(a) vs 95% water for coacervate III).

Properties of Coacervates. Coacervate prepared at $Y = 0.38$ and 22 °C for 1.41×10^5 (3 g/L) was separated from supernatant by centrifugation (1 h, 22 °C, 3700 rpm). Upon heating of the samples to 28 °C (see Scheme 1), both optically clear phases (S1 and C1) became turbid. This indicates a difference in composition between the supernatant and the original solution such that a new phase boundary is established, presumably with a higher LCST. In the absence of full analytical data, we can

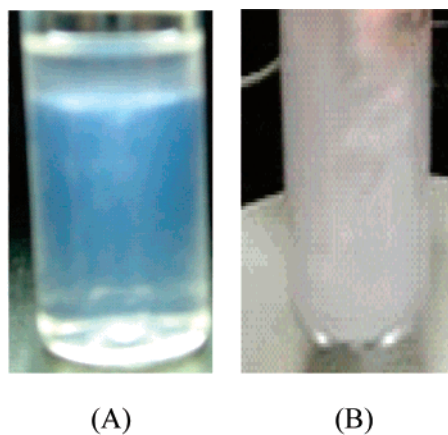


Figure 10. (A) Coacervate and supernatant C1C and C1S (see Scheme 1 and text for explanation). (B) Silky threads appearing in a coacervate prepared with PDADMAC $M_n = 4.60 \times 10^5$, $C_p = 1$ g/L, $I = 0.6$ M, and $Y = 0.7$ at 6 °C, brought to $T = 20$ °C with stirring.

merely report the concentrations of TX100 for coacervates and supernatant are 64 and 6 mM, respectively. Similarly, the initial coacervate upon heating forms a new biphasic system (Figure 10A). The volume fraction of the new coacervate from S1 (S1C) is less than that of the first coacervate (C1), and the volume of the new supernatant from the C1 (C1S) is smaller than the first supernatant (S1). There is clearly successive depletion of phase-separating material in these processes, but further analyses are required to establish the changes in composition.

The sensitivity of coacervate and supernatant layers formed at one temperature T_ϕ to further increase in temperature is manifested in the direct visualization of subtle temperature gradients as coexisting regions of turbidity (Figure 10B) whose presence also attests to the high viscosity of these systems. Somewhat similar gradients of turbid zones were seen under very low shear, e.g., from simple gravitational flow. These “silky” domains are reminiscent of the shear-banding reported by Pine and co-workers in systems of rodlike micelles, e.g., 10 mM solutions of salicylate salts of alkylammonium surfactants,^{45,46} in which “white” shear-induced phases (SIP’s) coexist with a transparent phase separated by stable interfaces on the 10–100 μm length scale. The same authors have reported shear-induced separation of semidilute polymer solutions into polymer-rich and polymer-poor domains.⁴⁷

Rodlike micelle systems entangle at low concentrations like polymers but also break and reform spontaneously. Ionic micelles approach rodlike dimensions when intramicellar repulsive forces among head groups are relieved by counterion binding. In this case, we propose that the polycation can function as a counterion, binding cooperatively to multiple anionic sites on the mixed micelles. Thus, a single polymer chain can bind a number of elongated micelles. Previous elemental analysis of a similar PDADMAC/TX100-SDS coacervate²² showed it to be 4% SDS, 8% TX100, 3.4% NaCl, and 4.4% PDADMAC w/w. Prepared in 0.6 M NaCl, that sample had a somewhat higher solids content (80% water vs 85% water here). Nevertheless, we can still assume that the PDADMAC concentration in coacervate B (Figure 2) prepared in region V(a) (Figure 1) is above the polymer overlap concentration, yielding an entangled but anisotropic system of polycation–micelle complexes. If these bound and elongated micelles are oriented under shear, a more dense structure can form along shear lines, similar to the dense phase formed when small ions are expelled upon an increase in temperature. Visual observations of air bubbles and some primitive measurements of capillary flow indicate that the

system slightly below T_ϕ is shear-thickening (agitation produces a gel-like state) but that the viscosity drops by a factor of 3 just above T_ϕ . This may indicate the alignment of polyelectrolyte–rodlike micelle complexes by shear to give an extended network, which is broken when thermally induced dense phases occur regionally throughout the system. Rheological and scattering experiments are currently underway to confirm these speculations.

Conclusions

Multiple phase transitions, strongly sensitive to temperature, ionic strength, polyelectrolyte MW, and micelle surface charge density, have been observed in the PDADMAC/SDS-TX100 system. These include the following: (a) noninteracting system \rightarrow soluble complex II; (b) soluble complex II \rightarrow coacervate III; (c) soluble complex IV \rightarrow coacervate III; (d) soluble complex IV \rightarrow coacervate V(a); (e) soluble complex IV \rightarrow precipitate. (Not observed but inferred is the transition from coacervate V(a) to precipitate.) Transitions b–e can be induced by temperature, but all systems exhibit an LCST below which no coacervation can occur. Coacervate densities increase with temperature or micelle charge densities. It seems likely that desolvation of coacervates is coupled to the entropically favored expulsion of counterions.

The coacervation domain is enhanced by increased polycation MW. Since coacervation is preceded by soluble aggregates, it appears likely that aggregate formation occurs more readily for higher MW interpolyion complexes. It also appears likely that coacervation will not occur below a critical MW. The opposite effect is observed for precipitation, which is enhanced by a decrease in MW. This may be ascribed to the greater significance of the loss of chain configurational entropy for precipitation.

The distinction between soluble complex II and soluble complex IV is well understood, but the difference between coacervate III and the more dense and viscous coacervate V(a) is currently unknown and interesting. On the basis of preliminary observations, it seems possible that transitions b–d are shear dependent. It is proposed that the high viscosity of coacervate V(a) can arise from entangled chains of polycation-bound micelles.

Acknowledgment. Support by Shiseido Corp. is acknowledged.

References and Notes

- (1) Tsuchida, E.; Abe, K. *Interactions Between Macromolecules in Solution and Intermacromolecular Complexes*; Springer-Verlag: Berlin, 1982.
- (2) Philipp, B.; Dautzenberg, H.; Linow, K.-J.; Kotz, J.; Dawydoff, W. *Prog. Polym. Sci.* **1989**, *14*, 91.
- (3) Veis, A. *J. Phys. Chem.* **1963**, *67*, 1960.
- (4) Kaibara, K.; Okazaki, T.; Bohidar, H. B.; Dubin, P. L. *BioMacromolecules* **2000**, *1*, 100.
- (5) Leisner, D.; Imae, T. *J. Phys. Chem. B* **2003**, *107*, 8078.
- (6) Wang, Y.; Kimura, K.; Huang, Q.; Dubin, P. L.; Jaeger, W. *Macromolecules* **1999**, *32*, 7128.
- (7) Wang, Y.; Kimura, K.; Dubin, P. L.; Jaeger, W. *Macromolecules* **2000**, *33*, 3324.
- (8) Goddard, E. D. *J. Soc. Cosmet. Chem.* **1990**, *41*, 23.
- (9) Shahidi, F.; Han, X. *Crit. Rev. Food Sci. Nutr.* **1993**, *33*, 501.
- (10) Mattison, K. W. Ph.D. Thesis, Purdue University, West Lafayette, IN, 1999.
- (11) (a) Swanson-Vethamuthu, M.; Dubin, P. L.; Almgren, M.; Li, Y. *J. Colloid Interface Sci.* **1997**, *186*, 414. (b) Sudbeck, E. A.; Dubin, P. L.; Curran, M. E.; Skelton, J. *J. Colloid Interface Sci.* **1991**, *142*, 512.
- (12) Strege, M. A.; Dubin, P. L.; West, J. S.; Flinta, C. D. *Protein Purification: Molecular Mechanisms of Large-Scale Processes*; ACS

Symposium Series 427; American Chemical Society: Washington, DC, 1990; pp 66–79.

- (13) Wang, Y.-f.; Gao, J. Y.; Dubin, P. L. *Biotechnol. Prog.* **1996**, *12*, 356.
- (14) Xia, J.; Mattison, K.; Romano, V.; Dubin, P. L.; Muhoberac, B. B. *Biopolymers* **1997**, *41*, 359.
- (15) Mishael, Y. G.; Dubin, P. L. *Environ. Sci. Technol.* **2005**, *39*, 8475.
- (16) Ray, B.; El Hasri, S.; Guenet, J.-M. *Eur. Phys. J. E* **2003**, *11*, 315.
- (17) Leonard, M. J.; Strey, H. H. *Macromolecules* **2003**, *36*, 9549.
- (18) Thunemann, A. F. *Prog. Polym. Sci.* **2002**, *27*, 1473.
- (19) (a) Wiegel, F. W. *J. Phys. A: Math. Gen.* **1977**, *10*, 299. (b) Odijk, T. *Macromolecules* **1980**, *13*, 1542.
- (20) (a) von Goeler, F.; Muthukumar, M. *J. Chem. Phys.* **1994**, *100*, 7796. (b) Kong, C. Y.; Muthukumar, M. *J. Chem. Phys.* **1998**, *109*, 1522.
- (21) Dubin, P. L.; Davis, D. *Colloids Surf.* **1985**, *13*, 113.
- (22) Dubin, P. L.; Rigsbee, D. R.; Gan, L. M.; Fallon, M. A. *Macromolecules* **1988**, *21*, 2555.
- (23) Rigsbee, D. R.; Dubin, P. L. *Langmuir* **1996**, *12*, 1928.
- (24) Fallon, M. M.S. Thesis, Purdue University, West Lafayette, IN, 1986.
- (25) Hahn, M.; Jaeger, W. *Angew. Makromol. Chem.* **1992**, *198*, 165.
- (26) Provencher, S. W. *Comput. Phys. Commun.* **1982**, *27*, 229.
- (27) Dubin, P. L.; Rigsbee, D. R.; McQuigg, D. W. *J. Colloid Interface Sci.* **1985**, *105*, 509.
- (28) Dubin, P. L.; Thé, S. S.; McQuigg, D. W.; Chew, C. H.; Gan, L. M. *Langmuir* **1989**, *5*, 89.
- (29) Li, Y.; Dubin, P. L.; Havel, A. H.; Edwards, S. L.; Dautzenberg, H. *Macromolecules* **1995**, *28*, 3098.
- (30) Veis, A.; Aranyi, C. *J. Phys. Chem.* **1960**, *64*, 1203.
- (31) Bungenberg de Jong, H. G.; Kruyt, H. R. *Kolloid Z.* **1930**, *50*, 39.
- (32) Bungenberg de Jong, H. G. In *Colloid Science*; Kruyt, H. R., Ed.; Elsevier: Amsterdam, 1949; Vol. I.
- (33) Oparin, A. I.; Gladilin, K. L.; Kirpotin, D. B.; Chertibrim, G. V.; Orlovsky, A. F. *Dokl. Acad. Nauk. SSSR* **1977**, *232*, 485.
- (34) Oparin, A. I. *Origin of Life*; Dover Publications: New York, 1953.
- (35) Overbeek, J. T.; Voorn, M. J. *J. Cell. Physiol. Suppl.* **1957**, *49*, 7.
- (36) Shultz, A. R.; Flory, P. J. *J. Am. Chem. Soc.* **1953**, *75*, 3888.
- (37) Flory, P. J. *Principals of Polymer Chemistry*; Cornell University Press: Ithaca, NY, and London, 1953; p 541.
- (38) Li, Y.; Dubin, P. L.; Dautzenberg, H.; Lück, U.; Hartmann, J.; Tuzar, Z. *Macromolecules* **1995**, *28*, 6795.
- (39) Dubin, P. L.; Thé, S. S.; Gan, L. M.; Chew, C. H. *Macromolecules* **1990**, *23*, 2500.
- (40) Dubin, P. L.; Principi, J. M.; Smith, B. A.; Fallon, M. A. *J. Colloid Interface Sci.* **1989**, *127*, 558.
- (41) Thé, S. S. M.S. Thesis, Purdue University, West Lafayette, IN, 1988.
- (42) Hollmann, O.; Gutberlet, T.; Czeslik, C. *Langmuir* **2007**, *23*, 1347.
- (43) Laugel, N.; Betscha, C.; Winterhalter, M.; Voegel, J.; Schaaf, P.; Ball, V. *J. Phys. Chem. B* **2006**, *110*, 19443.
- (44) Burgess, D. J. *J. Colloid Interface Sci.* **1990**, *140*, 227.
- (45) Boltenhagen, P.; Hu, Y.; Matthys, E. F.; Pine, D. J. *Europhys. Lett.* **1997**, *38*, 389.
- (46) Boltenhagen, P.; Hu, Y.; Matthys, E. F.; Pine, D. J. *Phys. Rev. Lett.* **1997**, *79*, 2359.
- (47) Migler, K.; Liu, C.; Pine, D. J. *Macromolecules* **1996**, *29*, 1422.